nature communications

Article

https://doi.org/10.1038/s41467-024-55494-2

Intrinsically stretchable fully π-conjugated polymers with inter-aggregate capillary interaction for deep-blue flexible inkjet-printed light-emitting diodes

Received: 10 October 2023

Accepted: 13 December 2024

Published online: 02 January 2025

Check for updates

Mingjian Ni[1,2], Zhiqiang Zhuo[1], Bin Liu[3], Xu Han[2], Jing Yang[1], Lili Sun[4], Yuekuan Yang[2], Jiangli Cai[3], Xiang An[1], Lubing Bai[1], Man Xu[5], Jinyi Lin[1,6] ✉, Quanyou Feng[5], Guohua Xie[2], Yutong Wu[1] & Wei Huang[1,2,3,4,5] ✉

Fully π-conjugated polymers consisting of plane and rigid aromatic units present a fantastic optoelectronic property, a promising candidate for printed and flexible optoelectronic devices. However, obtaining high-performance conjugated polymers with an excellent intrinsically flexible and printable capacity is a great challenge due to their inherent coffee-ring effect and brittle properties. Here, we report an asymmetric substitution strategy to improve the printable and stretchable properties of deep-blue light-emitting conjugated polymers with a strong inter-aggregate capillary interaction for flexible printed polymer light-emitting diodes. The loose rod-shaped stacking of asymmetric conjugated polymers chain in the precursor printed ink makes it easier to improve the intrinsic stretchability of inkjet-printed films. More interestingly, the anisotropic shape rod-like aggregate of conjugated polymers chains also induced a strong capillary interaction and further suppressed the coffee-ring effect, which is more likely to allow for uniform deposition during printed processing and form uniform printed films.

Emerging printed and flexible electronics technology provided a powerful engine to promote the development and innovation of modern electronic equipment, such as high-quality displays and large-area solid-light, bionics electronic skin, and parabrain circuits[1–5]. Flexible printed polymer light-emitting diode (FPPLED) is an essential component of flexible display equipment owing to their low-cost processing, potentially mechanical flexibility, and color tenability[6–10]. As the critical element in flexible display, the morphological uniformity and optoelectronic batch stability of printed light-emitting polymer layers is prerequisite to ensure their performance and excellent operational stability[11–14]. As a typical light-emitting polymer, traditional fully π-conjugated polymers (FπCPs) chains always easily tend to self-assemble into rigid and brittle semi-crystalline structure, due to strong face-to-face π-π interaction, which result into weak inter-chain entanglement with low viscosity in the precursor ink, and lead to the formation of coffee rings[15–17]. In fact, the ubiquitous nature of the coffee-ring effect has made it difficult to avoid in inkjet-printed processing of FπCPs for the fabrication of FPPLED[3,18,19]. The generation of coffee-

[1]Key Laboratory of Flexible Electronics (KLOFE) & Institute of Advanced Materials (IAM), Nanjing Tech University (NanjingTech), Nanjing, China. [2]The Institute of Flexible Electronics (IFE, Future Technologies), Xiamen University, Xiamen, China. [3]Henan Industrial Science & Technology Institute for Flexible Electronics, Henan University, Zhengzhou, China. [4]School of Flexible Electronics (SoFE) & State Key Laboratory of Optoelectronic Materials and Technologies, Sun Yat-sen University, Shenzhen, China. [5]State Key Laboratory of Organic Electronics and Information Displays & Institute of Advanced Materials (IAM), Nanjing University of Posts & Telecommunications, Nanjing, China. [6]Institute of Quantum and Sustainable Technology (IQST), School of Chemistry and Chemical Engineering, Jiangsu University, Zhenjiang, China. ✉e-mail: iamjylin@njtech.edu.cn; vc@nwpu.edu.cn; iamdirector@fudan.edu.cn

rings often results in uneven deposition of printed films, affecting the resolution of the patterns and the optoelectronic performance of the flat panel displays[3,4]. In addition, independent interchain aggregates produce uneven deposition by capillary flow, inducing the complicated photo-physics of the multi-chain excited species and altered the color purity and the emission efficiency, which is undesirable for the fabrication of deep-blue PLEDs[3,19–21]. Up to date, many physical and engineering strategies have been implemented to inhibit coffee rings, such as doping surfactants in solvents, using mixed viscous solvents, changing the substrate's surface energy, etc.[3,18,19,22] which is not suitable for the deep-blue large-area printed PLEDs because of their low capacity of defect tolerance. Therefore, rationally designing deep-blue emitting FπCPs to weaken the capillary flow during the evaporation process of ink droplets and suppress the formation of coffee rings is the key to realizing large-area deep-blue flexible PLEDs manufactured by inkjet printing.

In the printed processing, the weak inter-aggregate or intermolecular interactions caused a serious capillary flow outward from the center of the ink drop, bring suspended aggregate and molecules to the edge and form the coffee ring during evaporation proceeds (Fig. 1a)[23–25]. Interestingly, the anisotropic shape of the aggregate or particles significantly deforms interfaces, producing strong capillary interactions, which is beneficial for suppressing the formation of coffee ring (Fig. 1b)[22,26–28]. Besides, FπCPs with potential intrinsic viscoelasticity can reasonably weaken capillary flow through strong interchain entanglement and inhibit the formation of coffee rings, making them ideal candidate materials for printed electronic devices[18,19]. Therefore, obtaining the intrinsically viscoelastic FπCPs with an anisotropic shape aggregate is an effective strategy to obtain strong capillary interactions and avoid the coffee ring effect for printed and flexible optoelectronics applications. In this work, we use an asymmetric substitution strategy to design and synthesize intrinsically stretchable FπCPs with a strong inter-aggregate capillary interaction to fabricate flexible inkjet-printed deep-blue PLEDs (Fig. 1c). In solution, the anisotropic shape aggregate with a relatively loose stacking is more likely than dense Gaussian chain stacking to induce uniform deposition of polymers and form high-quality films during the evaporation of the solution (Fig. 1d). At the same time, this loose stacking makes it easier for the molecular chains to slip under the action of external force, resulting in the polymer having better tensile properties (Fig. 1e). Therefore, designing FπCPs with loose anisotropic aggregate is an effective strategy to prepare active layers for fully flexible inkjet-printed devices (Fig. 1f).

Results

Preparation and structural characterization of asymmetric FπCPs

In general, to precisely tune the morphological shape of interchain aggregates is an effective way to suppress the formation of coffee rings, which can be achieved by increasing the asymmetry degree of the polymer units[22]. This asymmetric substitution backbone structure can change the conformation and stacking mode of the molecular chain so that the polymer can be uniformly deposited during the volatilization process of the solution to form a high-quality film. It is worth noting that this asymmetric structure can also disrupt the long-range order structure of chains and further inhibit the formation of brittle crystallites, thereby improving their viscoelastic properties. Therefore, to improve the micro-domain structure of the film by introducing substituents on one or both sides of the polymer unit is an effective way to improve the inkjet-printed capacity and intrinsically flexible properties. First, traditional Yamamoto polymerization is introduced here to prepare the PFPO with a one-side asymmetric substitution at fluorene 9-site and POPOF with a double-side asymmetric substitution at fluorene 4, 9-sites (Fig. 1c and Supplementary Figs. 1–2). Meanwhile, PODPF was synthesized as a comparative material according to our previous report. Then, their molecular structures were effectively confirmed by NMR spectroscopy (Supplementary Figs. 3–12). Their number-average molecular weights (M_n) were estimated by gel chromatography to be 75 kDa (PFPO), 36 kDa (POPOF), and 60 kDa (PODPF), respectively (Supplementary Fig. 13). Thermodynamic analysis (Supplementary Fig. 14) showed that the decomposition temperature (T_d) of both PFPO and POPOF was 342 °C, showing good thermal stability, attributed to their similar backbone structure. In addition, as the proportion of rigid benzene rings in the molecular chain decreases, their glass transition temperatures (T_g) gradually decrease, which are 213 °C (PODPF), 130 °C (PFPO), and 87 °C (POPOF), respectively. To a certain extent, lower T_g may reveal the easily interchain slippage, which is beneficial to enhance their inherent flexibility.

Printable capacity of the model asymmetrically substituted FπCPs

In general, the printable capacity of semiconductor ink is a key factor to dominate the surface morphology and optoelectronic property of the printed films, which can further affect printed electronic devices' performance and stability. The ubiquitous coffee-ring effect that appears in ink droplets directly affects the quality of the film and the performance of the device. We systematically characterized the inkjet film-forming ability of PFPO and POPOF (Fig. 2). In the process of inkjet printing, the stable ejection of ink droplets plays a pivotal role in enhancing the film quality. The polymer toluene solution with a concentration of 5 mg mL^{-1} was prepared to ensure the smooth extrusion of the ink. Then, the inks viscosity and surface tension of PODPF, PFPO, and POPOF were characterized to be 0.01, 0.04, 0.007 Pa·s and 25.5, 25.9, and 26.4 mN m^{-1}, respectively (Fig. 2a, Supplementary Figs. 15–16). It is worth noting that the viscosities of three ink remain below 0.05 Pa·s, which is beneficial to the stable ejection of the ink and the spread on the substrate. The surface tension of the ink increases with the proportion of polymer alkyl chains increases. The moderate surface tension benefits the hovering of ink droplets in the air and suppresses the tailing phenomenon produced during the falling of ink droplets.

Subsequently, we further explored the printed inkjet property on the PEDOT:PSS film. We first explored the contact angles of three polymer inks on PEDOT:PSS films (Supplementary Fig. 17). The contact angles of PODPF, PFPO, and POPOF were 8.8°, 14.1°, and 10.8°, respectively. This good wettability is crucial for achieving a uniform printing film. Then, the M-type pulse voltage was used for inkjet printing on the PEDOT:PSS films (Supplementary Fig. 18). To further investigate the printed film morphology, the surface morphology of ink droplets was characterized by atomic force microscopy (AFM) and fluorescence microscopy (Fig. 2c). The diameters of the three single ink droplets were 85, 83, and 90 μm (Fig. 2b), which are closely associated with the ink viscosity. However, PODPF printed film exhibits severe coffee-ring under fluorescence microscopy (Fig. 2c). In order to deeply characterize the uniformity of the film, the coffee-ring degree is defined as CRF = H_{min}/H_{max}, where H_{min} and H_{max} are the minimum and maximum thickness of the printed film, respectively. The CRF values of PODPF, PFPO, and POPOF are calculated at about 0.04, 0.90, and 0.86, respectively (Fig. 2b). The CRF value of PFPO and POPOF is 20 times than that of PODPF, and the film uniformity is better than that of PODPF. In fact, PODPF has a strong π-π interaction and an excellent crystallization capacity, which caused the formation of densely stacked semi-crystalline aggregate in the ink. This tight aggregate in ink droplets is easily migrating toward the edges of the droplets, creating coffee rings. However, both PFPO and POPOF are relatively loosely stacked in ink droplets, which is beneficial to suppress the coffee-ring effect.

In order to verify the above conjecture, light scattering experiments were conducted to explore the dynamic aggregation behavior

https://doi.org/10.1038/s41467-024-55494-2

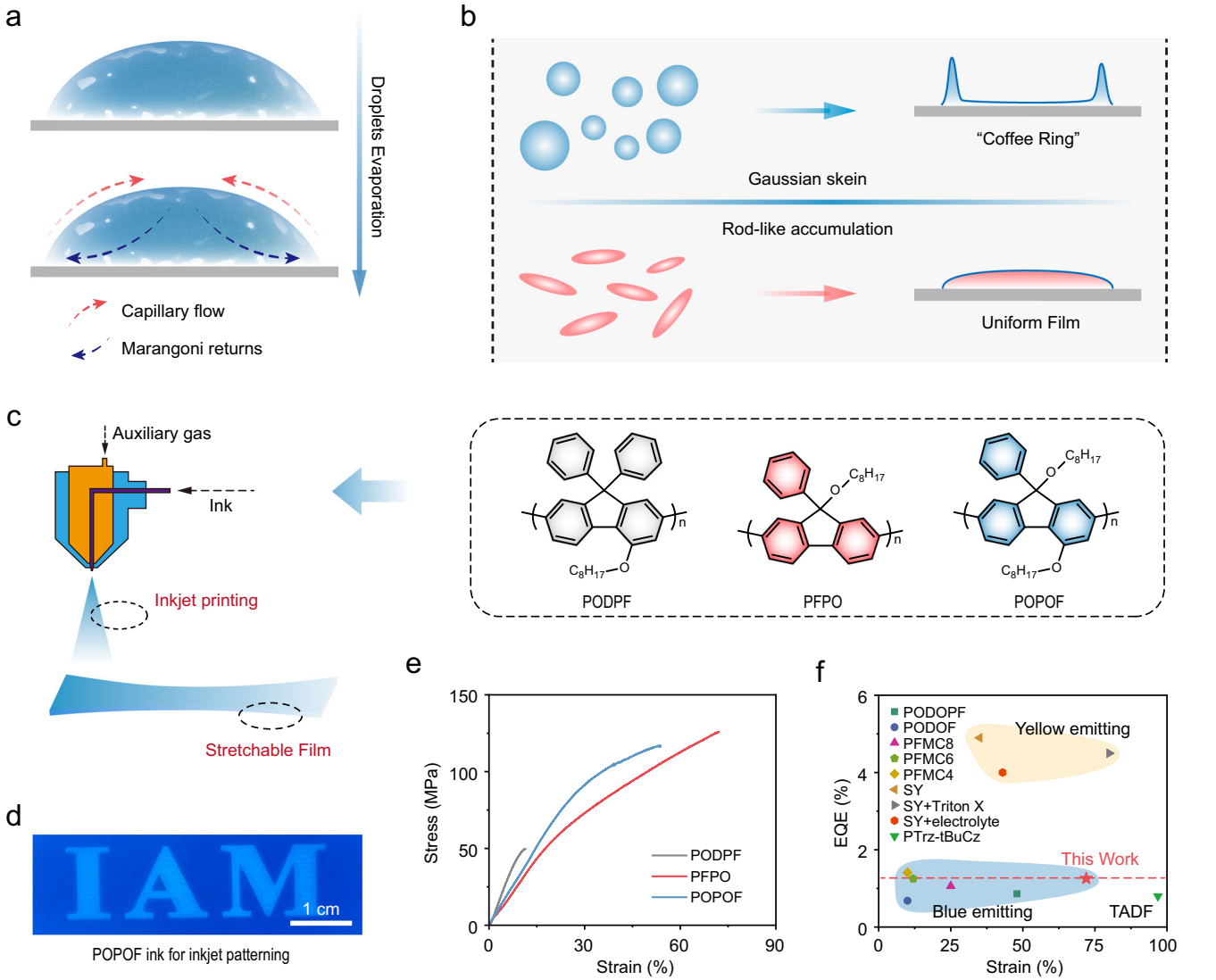

Fig. 1 | Molecular design of asymmetrically substituted FπCPs with an anisotropic shape aggregate toward suppressing coffee-ring effect in inkjet-printed processing. a Molecular motion during evaporation of printed ink droplets; **b** The Gaussian coils stack in the molecular chain will aggravate the formation of coffee rings. This article uses the anisotropic shape rod-like aggregate of FπCPs chains to suppress the coffee-ring effect; **c** Chemical structures of asymmetrically substituted random copolymers FπCPs (PODPF, PFPO, and POPOF); **d** Fluorescence microscopic images of POPOF inkjet printing pattern (under UV lamp 365 nm) on flexible PET substrate; **e** The stress-strain curve of three films was obtained under room temperature with a stretching rate of 0.005 mm s^{-1}; **f** Comparison of the EQE and stretchability given by PFPO (this work) with the corresponding values for previously reported intrinsically stretchable light-emitting polymers based on fluorescence emitters[8,31,37,38].Source data are provided as a Source Data file.

of polymer chains in printed ink. As shown in Figs. 2d, S19, the three polymers present a diverse aggregation behavior in the precursor ink with high concentration (5 mg ml^{-1}). The R_h of their aggregated peaks are 44 nm, 146 nm, and 185 nm, respectively. The R_h at 1–10 nm is attributed to their single-chain behavior, which is consistent with the R_h of their single-chain in dilute solutions. Subsequently, SLS experiments were used further to characterize the inter-chain stacking mode in the aggregate. The fractal dimension (d_f) is an important parameter to probe the tightness of interchain stacking, that the high value also indicated the denser interchains stacking (Fig. 2e). The d_f values of PODPF, PFPO, and POPOF are estimated to be 1.43, 1.19, and 0.7, respectively, which means that PODPF chain showed the densest stacking among these polymers. Normally, when the d_f value = 1.78, the chain is ideally considered to exhibit an isotropic Gaussian coil stacking model[29,30]. When the d_f value = 1, the molecular chain shows an anisotropic rod-like stacking structure. Therefore, the chains of PODPF are closer to the Gaussian coil stacking model. At the same time, PFPO and POPOF are closer to the anisotropic shape rod-type stacked aggregate. The looser interchain stacking and stronger inter-aggregate capillary interactions are more conducive to inhibiting the formation of coffee rings than the densely stacked Gaussian coil structure. Interestingly, the change in stacking density also explains their difference in mechanical properties. The looser the molecular chains are stacked, the easier the molecular chains slide, resulting in a decrease in modulus[31]. Therefore, PFPO has the best potential tensile properties. In addition, the nanostructure of large-area printed films was characterized by AFM (Supplementary Fig. 20). According to the results, the RMS of the PODPF printed film is 11.9 nm, which is much larger than its spin-coated film. PFPO and POPOF have similar RMS (PFPO = 0.547 nm, POPOF = 1.21 nm), which are close to those of the spin-coated films. This change mainly comes from the difference in their ability to inhibit the coffee ring. Therefore, PFPO and POPOF have more suitable printable capacity for the fabrication of the inkjet-printed optoelectronic devices.

https://doi.org/10.1038/s41467-024-55494-2

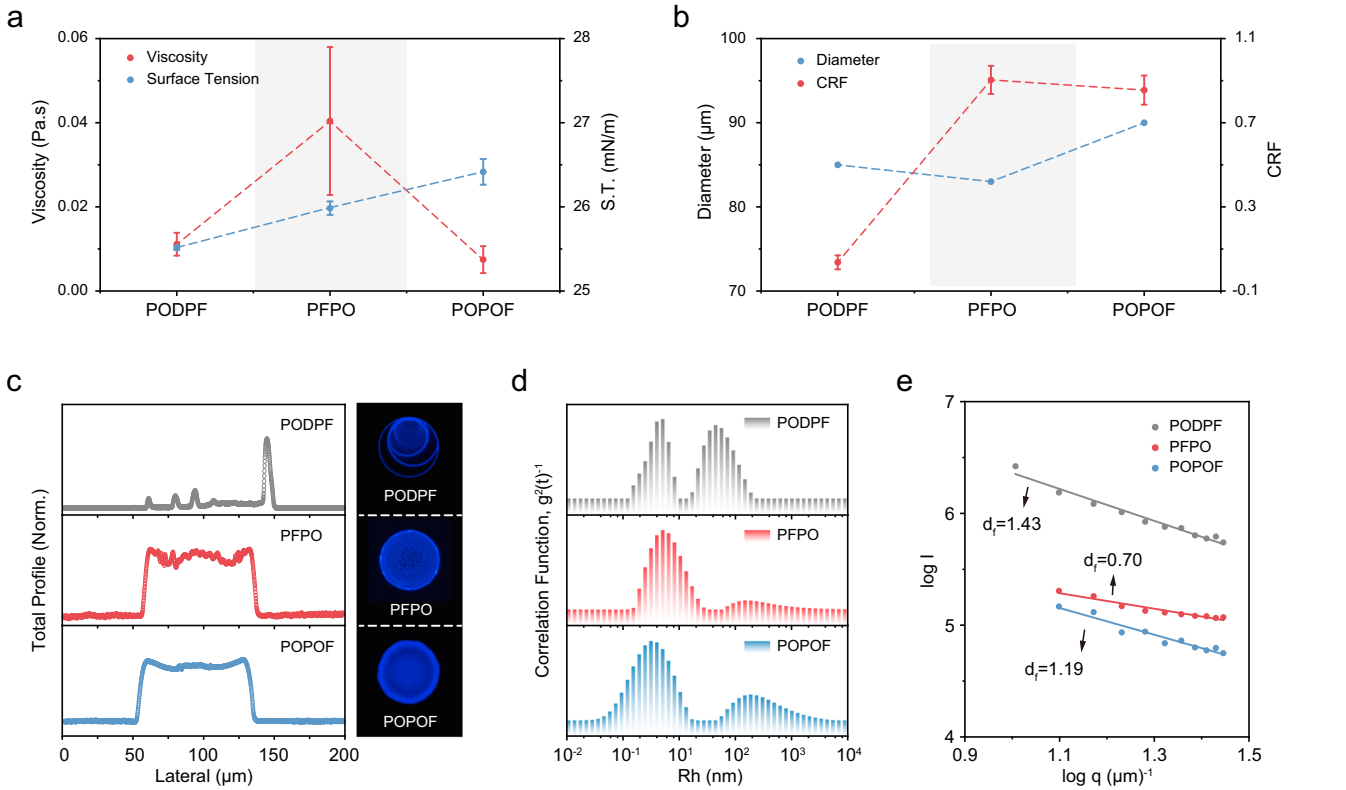

Fig. 2 | Inkjet printable capacity of three models asymmetrically substituted FπCPs. a Viscosity and surface tension of PODPF, PFPO, and POPOF inks (data are represented as mean values ± s.d.); **b** Diameter and coffee ring degree of inkjet films for PODPF, PFPO, and POPOF (data are represented as mean values ± s.d.); **c** Atomic force microscopy characterization and the fluorescence microscopy of individual ink droplets; LS results of three ink (toluene, 5 mg mL^{-1}): R_h distribution (**d**), log $I_{(q)}$-log q curves (**e**). Source data are provided as a Source Data file.

Intrinsically mechanical properties of the model asymmetrically substituted FπCPs

As mentioned above, the asymmetric substitution of FπCPs can change the stacking mode of molecular chains and reduce the long-range ordered crystallization in the films[32,33], thereby improving their mechanically flexible properties. To confirm our conjecture, we performed the intrinsically mechanical analyses of three polymers. Usually, the chain behavior in precursor solution can not only dominate the structural development during film casted processing but also impact their mechanical properties. Therefore, light scattering experiments are probed to explore the chain behavior of three FπCPs in solutions (1 mg mL^{-1}). As shown in Fig. 3a, b, PFPO and POPOF have only one hydrodynamic radius (R_h), which is 5.08 nm and 3.15 nm, attributed to their single-chain behavior in solution. However, even at low concentrations, PODPF showed a strong tendency to aggregate (R_h = 10.54 nm, R_h = 56.48 nm), which may be caused by interchain π-π interaction. Such aggregates not only hinder the accurate determination of the size and properties of polymer single chains, but also strongly affect the film quality and mechanical properties of polymers. The roughness-mean-square (RMS) of the PODPF spin-coated film is 0.71 nm, while the RMS of PFPO and POPOF are only 0.35 and 0.37 nm (Supplementary Fig. 20). To further explore the single-chain behavior, the persistence length (l_{ps}) of PFPO and POPOF was deduced by the formula:

$$R_g^2 \cdot 3 \cdot M_0 = l_{ps} \cdot l_0 \cdot M \quad (1)$$

where l_0 is the length of the monomer, M_0 is the molecular weight of the monomer, M is the molecular weight of the polymer chain, and R_g is the root mean square radius of gyration (PFPO = 18.38 nm, POPOF = 12.99 nm, obtained by Static Light Scattering, SLS). As shown in Fig. 3c, the l_{ps} of PFPO and POPOF are estimated at about 6 nm and 8 nm, revealing the semi-rigid chain state. Compared with POPOF, PFPO has smaller l_{ps} due to the single-side substitution. This is because the interaction between side chains of PFPO makes the main-chain more likely to bend and form a ring structure, while the main chain of POPOF with double-side asymmetric substitution tends to be a straight chain[32,33]. Smaller l_{ps} means also indicates more flexibility of main-chain. Therefore, PFPO films have an excellent potentially flexible property.

Subsequently, we performed a mechanical analysis of the polymer films to confirm the above conjecture. First, the three polymer films were adhered to the PDMS substrate and stretched to observe the initiation and propagation of cracks in the film. As shown in Fig. 3d and Supplementary Fig. 21, PFPO and POPOF coated film have a similar crack initiation strain of 40%, but PODPF is only 10%. In addition, their elongation at break also showed the same trend (Figs. 1e, 3d), with PODPF only stretched to 11%, while PFPO and POPOF had elongation at break of 72% and 53%, five times than PODPF. This is at the forefront of intrinsically stretchable conjugated polymer emitters (Fig. 1f). The increased crack initiation strain and elongation at break of PFPO and POPOF indicates that asymmetric substitution is an effective method to improve the mechanically stretchable properties of FπCPs. In order to quantitatively analyze their mechanical properties, Nano-indentation was performed under constant displacement and constant load. As shown in Fig. 3e, the modulus and hardness of PODPF is larger than that of PFPO and POPOF, which verifies the correctness of our molecular design. On this basis, at a constant displacement of 60 nm, the maximum stress endured by PODPF is 73 μN, and the stresses of PFPO and POPOF are 48 μN and 50 μN, respectively (Fig. 3f). During the rebound process, PODPF and POPOF have similar rebound rates of 66% (40 nm), while PFPO has a rebound rate of 81% (51 nm).

https://doi.org/10.1038/s41467-024-55494-2

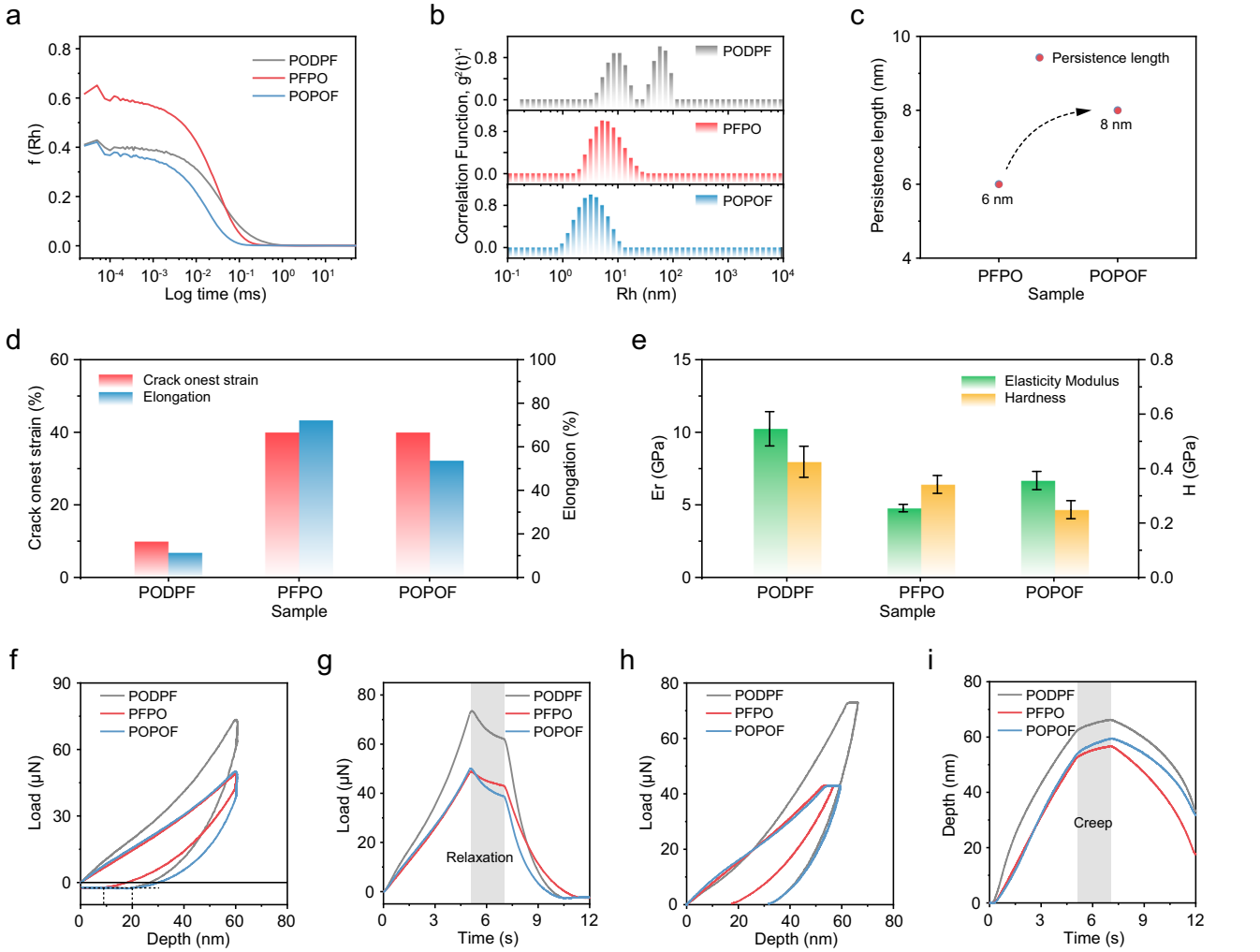

Fig. 3 | Chain behavior and intrinsic mechanical properties of model FπCPs. LS results of three polymers: normalized intensity correlation function ($g^2_{(t)}{}^{-1}$) (**a**), R_h distribution (**b**); **c** l_{ps} of PFPO and POPOF; **d** Elongation at break and crack initiation strain; **e** Young's modulus and hardness measured at the constant displacement mode; Load-depth curves (**f**) and load–time curves (**g**) in constant displacement; Load-depth curves (**h**) and depth–time (**i**) curves obtained at the constant load mode. Source data are provided as a Source Data file.

These results show that PFPO is the easiest to rebound and has the best elasticity, which may be attributed to its smaller l_{ps} and curved main-chain conformation. In the constant displacement mode, after relaxation for 2 s (Fig. 3g), the stresses of PODPF, PFPO, and POPOF were reduced by 15% (11 μN), 12% (6 μN), and 24% (12 μN), POPOF had the best ability to relax. In addition, their creep capabilities have a similar trend (Fig. 3h, i). After a creep time of 2 s, PODPF and PFPO have similar creep degrees, which are 6% (4 nm) and 7% (4 nm), respectively, while the creep of POPOF is 11% (6 nm). These results show that POPOF is most prone to creep and relaxation among the viscoelastic behaviors and has the best viscosity. Therefore, we concluded that unilateral asymmetric substitutions allow for excellent elasticity, which is more conducive to achieving the elastic behavior of the film. In contrast, bilateral asymmetric substitution gives the advantage of high viscosity to enhance the creep and relaxation ability. The above observations show that asymmetric substitution can improve the flexibility of FπCPs.

Photophysical characterization of the model asymmetrically substituted FπCPs

The interchain arrangement and stacking mode of FπCPs significantly influence their photophysical process and charge transport ability. We further studied the photophysical properties of these asymmetrically substituted FπCPs in solutions and films (Summarized in Table S2). As shown in Fig. 4a, PFPO and POPOF showed a similar absorption spectral profile with a maximum absorption peak at 395 nm and 403 nm in dilute solutions, attributed to their similar backbone structures. Similarly, PFPO and POPOF coated films have maximum absorption peaks at 390 and 396 nm, respectively. Subsequently, in-situ coated-time dependent PL spectra of PFPO and POPOF are explored here to explore the emission behavior of solution-solid states under solvent evaporation in the printed processing (Supplementary Fig. 22). As shown in Fig. 4a, both PFPO and POPOF diluted solutions have similar PL spectral shapes (PL_{PFPO} = 417, 442, 474 nm; PL_{POPOF} = 430, 458, 492 nm), three characteristic emission peaks attributed to the 0-0, 0-1, and 0-2 intrachain singlet transition. As we expected, PFPO and POPOF spin-coated film also displayed three characteristic peaks (PFPO = 425, 452, 483 nm, POPOF = 435, 463, 495 nm), the 0-0 peak of POPOF red-shifted about 5 nm, due to introduce the methoxy group at 4-sites causes the intrachain electron delocalization, also confirmed by the calculation of natural charge distribution (Supplementary Figs. 23–24). In addition, both two materials showed an excellent stable deep-blue emission after thermal annealing and air aging (Supplementary Fig. 25). As the energy dissipation center in PFPO and POPOF stretchable film, the anisotropic stacking also can

https://doi.org/10.1038/s41467-024-55494-2

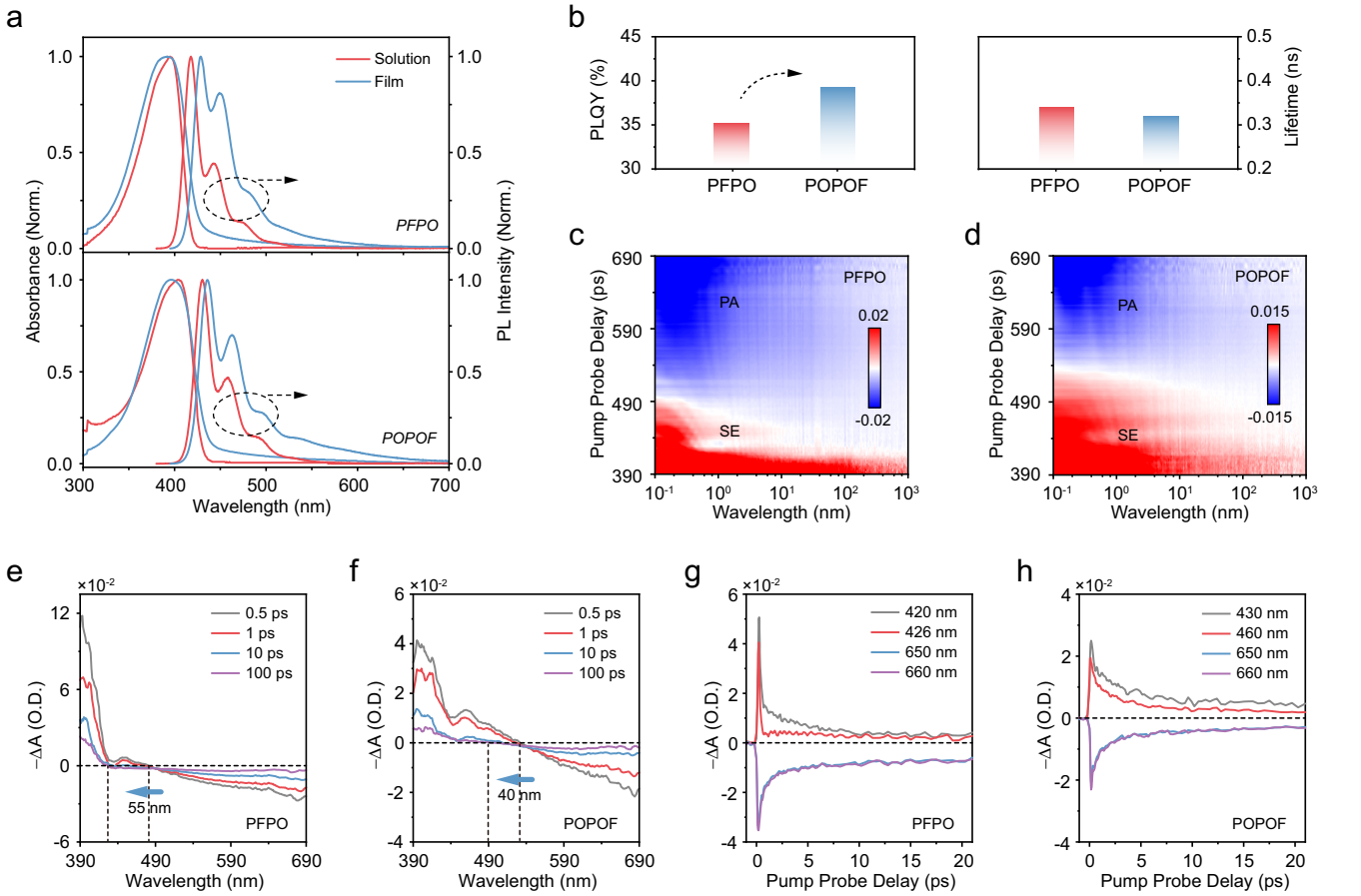

Fig. 4 | Photophysical properties of PFPO and POPOF. a Absorbance and PL spectra of two polymers in toluene solution (10^{-5} mg mL^{-1}) and spin-coated films. **b** Summary of quantum efficiency and lifetime of two polymer coated films. **c**, **d** Corresponding transient absorption contour plots. Transient absorption spectra were collected at different delay times after excitation (**e**, **f**) and their pump-probe kinetics at the selected wavelength (**g**, **h**). Source data are provided as a Source Data file.

suppress interchain aggregation to inhibit the electronic coupling between chromophores and the formation of excited states. In order to obtain the radiative and non-radiative transition rate transition rate, the quantum efficiency and lifetime of the film were characterized (Figs. 4b, S26). The quantum efficiencies of PFPO and POPOF coated films were 35.19% and 39.21%, respectively. Similar to the results discussed above, double-sided substitution makes the main chains tend to be straight, which is more likely to inhibit the electronic coupling between chromophores and the formation of excited states than the cyclic chain[33]. Therefore, the quantum efficiency of POPOF is higher than that of PFPO, and the radiative transition rate is higher (PFPO = 1.04 s^{-1}, POPOF = 1.23 s^{-1}). Subsequently, their excitonic dynamic behavior was studied by transient absorption spectroscopy (TA). As shown in Fig. 4c, d, both PFPO and POPOF exhibit obvious stimulated emission (SE, -ΔA > 0) and excited state absorption (PA, -ΔA < 0) signals. According to the differential transmission spectrum display (Fig. 4e, f), their signals gradually attenuate, and the zero-crossing point (-ΔA = 0) shows a blue shift with the delay time increases. PFPO has a blue shift of about 55 nm, and POPOF is blue-shifted by 40 nm, attributed to the change in intrachain conformation between the excited and ground states. It is further proved that double-sided substitution can inhibit the formation of long-lived polarons, thereby improving exciton utilization. Furthermore, the time decay dynamics of SE and PA show that the decay curves of POPOF have higher symmetry along the *x*-axis (Fig. 4g, h), further confirming their intramolecular singlet excitons in the solid state.

Optoelectronic properties of flexible inkjet-printed PLEDs

Excellent printed capacity, emission behavior, and intrinsic stretchability of the model asymmetric FπCPs are predicated on their potential application in flexible and printed electronic devices. Therefore, preliminary flexible PLEDs based on the PFPO and POPOF were manufactured via inkjet printing technology. Firstly, according to the cyclic voltammetry (CV) (Supplementary Fig. 27), the lowest unoccupied molecular orbital (LUMO) and highest occupied molecular orbital (HOMO) are −2.33 eV and −6.15 eV for PFPO, −2.40 eV and 5.97 eV for POPOF, respectively. Subsequently, PFPO and POPOF flexible inkjet-printed PLEDs were prepared on flexible PEN substrates with the device structure: ITO/PEDOT: PSS (40 nm)/EML (≈ 45 nm)/TPBi (25 nm)/LiF (0.8 nm)/Al (100 nm). As shown in Fig. 5a, both EL spectra of PFPO and POPOF-based PLEDs consisted of three feature emission peaks (EL_{PFPO} = 427, 445, 480 nm; EL_{POPOF} = 436, 458, 490 nm), attributed to their 0-0, 0-1, and 0-2 transition of main-chain singlet states. As expected, no obvious green-band emission appeared with increasing applied voltages, which also confirmed their stable deep-blue emission. Meanwhile, the turn-on voltages (V_{on}) of PFPO and POPOF-based inkjet PLEDs were 4.4 V and 4.0 V. The maximum brightness is about 1500 cd m^{-2} at 6.8 V and 3100 cd m^{-2} at 6.8 V for printed PLEDs based on PFPO and POPOF (Fig. 5b). Corresponding CIE coordinates are about (0.16, 0.07) and (0.17, 0.10), respectively (Supplementary Fig. 28a). Compared with PFPO, POPOF device has a lower V_{on} and higher brightness. This is because the interactions between adjacent side chains of PFPO cause the ring-like bent chain behavior, which is bad

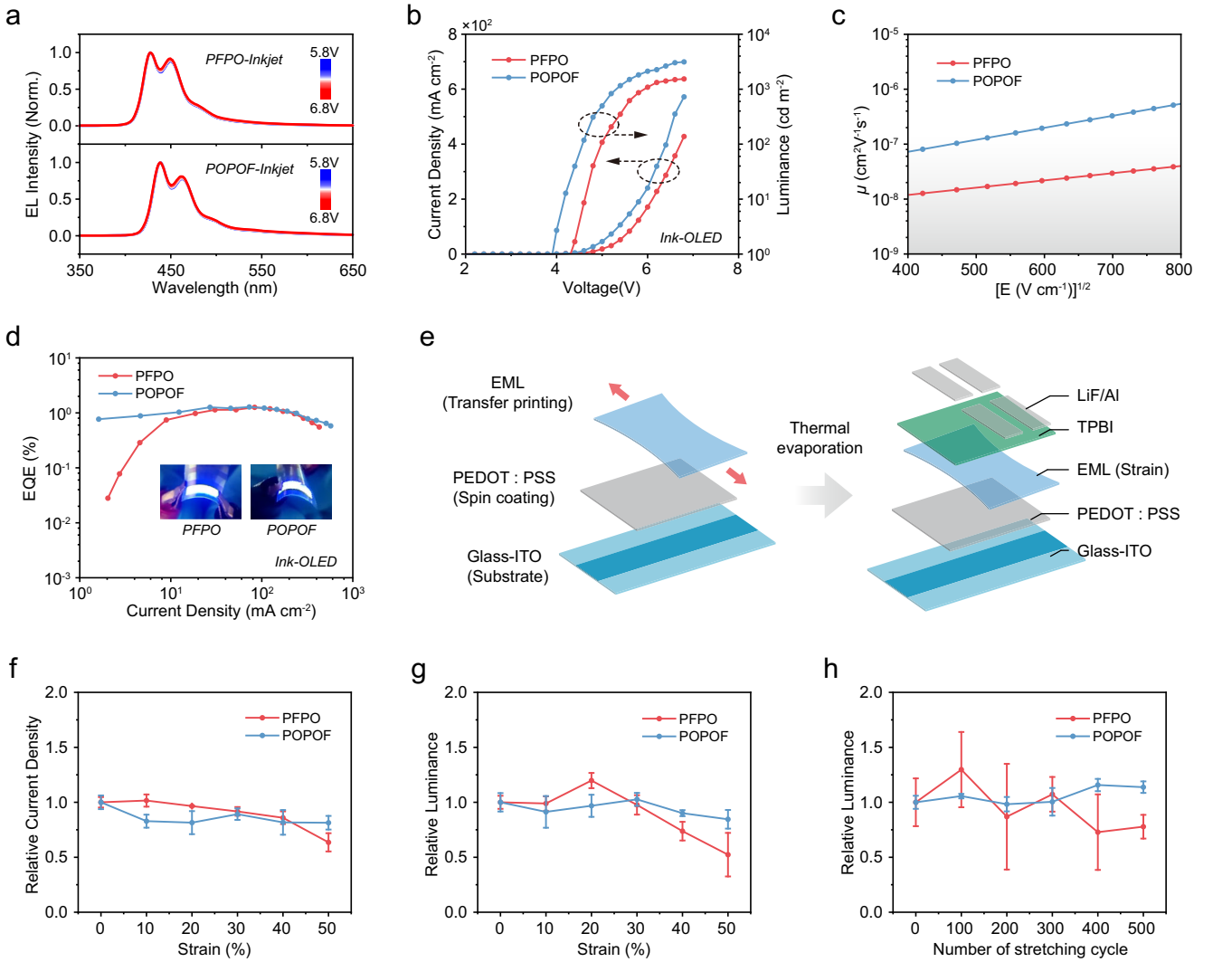

Fig. 5 | Performance of PFPO and POPOF-based flexible inkjet-printed PLEDs. **a** EL spectra of inkjet-printed PLEDs at different applied voltages. **b** J-V-L curves of corresponding inkjet-printed PLEDs. Carrier mobility characterization (**c**) and EQE (**d**) of inkjet-printed PLEDs. Insets are optical photos of their flexible device prepared by inkjet printing. **e** Schematic diagram of preparation of emitting layer stretching device. Maximum current density (**f**) and luminance (**g**) statistics of PLEDs using PFPO and POPOF films with increased strain (data are represented as mean values ± s.d.). **h** Relative highest luminance statistics of PLEDs using PFPO and POPOF films with cyclic strain (data are represented as mean values ± s.d.). Source data are provided as a Source Data file.

for the charge transport along the main-chain direction[32–34]. At the same time, the loose stacking of PFPO molecular chains limits the interaction and charge transfer between molecular chains, leading to a decrease in electric performance[35,36]. On the contrary, POPOF inhibits the formation of the ring-like main chain and enhances the charge transport ability. Therefore, as shown in Fig. 5c and Supplementary Fig. 29, in the range of the square root of the electric field ($E^{1/2}$) of 400–800 (V cm^{-1}) $^{1/2}$, the hole mobility of the PFPO is ≈ 10^{-8}·cm^2·V^{-1}·s^{-1}, which is one order of magnitude lower than that of POPOF (≈ 10^{-7}·cm^2·V^{-1}·s^{-1}). In addition, their external quantum efficiencies (EQE) and current efficiencies of corresponding PLEDs also showed the same trend, as shown in Fig. 5d, the maximum external quantum efficiencies of PFPO and POPOF-based PLEDs are 1.26% and 1.28%, respectively. This is at the forefront in terms of intrinsic stretchable blue fluorescent emitters (Fig. 1f). The maximum current efficiencies of PFPO and POPOF-based PLEDs are 0.74 and 1.14 cd A^{-1}, respectively (Supplementary Fig. 28b). It is worth noting that the performance of inkjet devices has reached a level comparable to that of spin-coated devices. As shown in Supplementary Fig. 30, the EQE of devices based PFPO and POPOF spin-coated films are 1.09% and 1.39%, attributed to subtle changes in film roughness.

In general, the intrachain conformation and interchain stacking mode of FπCPs are changed under stretched processing, which can also affect the device performance. Subsequently, to confirm the practical application of PFPO and POPOF in intrinsically stretchable PLEDs, PLEDs based on emission layer with different stretching degrees were prepared using transfer printing technology (Fig. 5e)[7]. As shown in Supplementary Fig. 31, both PFPO and POPOF devices exhibit excellent spectral stability as the strain increases, that is crucial for flexible PLEDs. Additionally, the strain-brightness-current density curves are shown in Fig. 5f, g and Supplementary Fig. 32. Meanwhile, the current density of PFPO device is almost constant at low strain but exhibits a slow decline at high strain, attributed to subtle defects generated in the PFPO film at high strain. Interestingly, brightness of PFPO increases at low strain, reaching a maximum of 800 cd m^{-2} at 20% stretch. This is attributed to a more balanced carrier injection and improved interface contact[7]. Subsequently, brightness of PFPO device shows a decreasing trend due to a reduction in the effective emitting area caused by the generation of subtle defects in the film. It is worth noting that at 50% stretch, there is a good stability for the current density and brightness of POPOF devices. To study the strain stability of PLED, we conducted cyclic stretching experiments on PFPO and

POPOF films under reasonable strain (15%) and prepared devices. As shown in Fig. 5h, after 500 cycles of strain, the brightness of the PFPO device first rose slightly and then began to decline, which may be due to the change in charge transfer caused by the change in chain conformation. In contrast, POPOF devices have better cyclic strain stability, the brightness of the POPOF device remained almost unchanged, and the EQE (Supplementary Fig. 33) also maintained at a relatively stable level. These results further effectively support the assumption that the denser interchain stacking and the inhibition of cyclic main chain formation in POPOF printed film can enhance charge transfer capabilities and present the superior stretch stability of optoelectronic performance.

Discussion

In summary, we demonstrated the asymmetric substitution strategy to prepare intrinsically stretchable deep-blue light-emitting FπCPs with a strong inter-aggregate capillary interaction for flexible inkjet-printed PLEDs. This asymmetric substitution strategy can disrupt chain regularity and ordered crystallization capacity of FπCPs, and is favorable for obtaining excellent stretchable properties to enhance the device deformation stability. PFPO with the one-side asymmetrically substitution has a smaller l_{ps} (6 nm), indicating good chain flexibility. Meanwhile, compared to the dense isotropic Gaussian chain stacking, loose anisotropic rod-shaped aggregate with a strong capillary interaction is more likely to present a uniform printed deposition of asymmetric PFPO and POPOF, which is beneficial for the formation of high-quality printed films. More interestingly, the elongation at break of freestanding POPOF and PFPO films reached 53% and 72%, much higher than PODPF (11%), indicating their good intrinsic stretchability. Flexible printed deep-blue PLEDs were also fabricated with a CIE of (0.17, 0.10), with comparable performance to that of spin-coated devices. Therefore, the asymmetric substitution strategy is effective for constructing printable flexible FπCPs for optoelectronic applications.

Methods

Materials

Reagent and catalysts used in the process were commercially available and used without further purification unless otherwise noted. 2,2′-bipyridine, 1,5-cyclooctadiene (COD) and bis(1,5-cyclooctadiene)nickel (0) ($Ni(COD)_2$) were purchased from Sigma-Aldrich. All other drugs mentioned in the synthesis process are derived from *Adamas-beta*. Dimethylformamide (DMF) was dried over calcium hydride (CaH) and distilled under a dry nitrogen atmosphere immediately prior to use. Toluene was dried over Na and distilled under a dry nitrogen atmosphere immediately prior to use. Anhydrous THF (HPLC grade) was collected from Solvent Purification Systems (Innovative Technology, Inc.). PEDOT:PSS (Clevios PVP AI 4083) was purchased from Heraeus Epurio (Germany). The synthesis of PFPO and POPOF are provided in the Supplementary Information.

Characterization

Absorption spectra were measured with a Shimadzu UV-1750 spectrometer at room temperature, and emission spectra were recorded on a Hitachi F-7100 luminescence spectrometer. Nanosecond time-resolved studies were performed with an Edinburgh FLS 1000 time-correlated single photon-counting (TCSPC). The quantum yield was measured by C11347 spectrometer (Hamamatsu, Japan). Cyclic voltammetric (CV) studies were taken using a CHI660C Electrochemical Work station in a three-electrode cell. The film morphologies of polymer films were measured with AFM in tapping mode with a Si tip (resonance frequency: 320 kHz; spring constant: 42 N/m) at a scanning rate of 1 Hz (Bruker's Dimension Icon). The dynamic light scattering (DLS) and static light scattering (SLS) measurements were carried out using an ALV/CGS-3. The nano-indentation test was carried out using a Hrysitron TI premier. Inkjet printing was tested using DB300 (Prtronic) at room temperature. The dynamic inkjet process adopts an M-shaped pulse waveform.

Structural characteristics via NMR technologies

The bruker 400 MHz Fourier Transform NMR spectrometer was used to obtain ^{1}H and ^{13}C NMR spectra at a frequency of 400 MHz and 100 MHz, respectively, at 20 °C. The coupling constants are expressed in Hz as a J value. The 90° pulses and a relaxation delay of 1 s were employed to record ^{1}H NMR spectra with a spectral width of 12.02 ppm and 128 scans.^{13}C NMR spectra were recorded using 45° pulse sequence with power-gated decoupling for suppression of the scalar couplings with protons, a spectral width of 236 ppm, 1024 scans, and a relaxation delay of 1 s. The values of chemical shifts are represented by δ in units of parts per million (ppm) relative to an internal standard [^{1}H NMR: tetramethylsilane (TMS) = 0.00 ppm] or relative residual peaks (^{1}H NMR: 7.26 ppm for $CDCl_3$;^{13}C NMR: 77.0 ppm triplet for $CDCl_3$). Briefly, the multiplicities of each signal peak are represented as s (singlet), d (doublet), t (triplet), q (quartet), dd (doublet of doublets), dt (doublet of triplets), and m (multiplet).

Fabrication of PLED

The ITO substrate was cleaned in an ultrasonic bath with detergent, acetone, isopropanol and deionized water, and treated with ultraviolet ozone for 10 min. Followed by spin coating of a PEDOT:PSS (AI 4083) solution at 3000 rpm for 45 s in air, and subsequent annealing at 120 °C for 10 min. The thickness of AI 4083 was around 40 nm. Then, the emitting layer was spin-coated from Tol solution (8 mg/mL) and annealed at 120 °C for 15 min in nitrogen-filled glovebox. Finally, the residue layers, such as 25 nm TPBi, 1 nm LiF and 100 nm Al, were deposited by thermal evaporating sequentially through a shadow mask at a pressure below 1×10^{-5} mbar. The area of the device was 4 mm^2 defined by the overlap between the ITO and Al electrode.

Fabrication of OLED devices with stretchable polymer films under stretching

For pre-stretched polymer films with different strains, Polymer film coated on OTs Glass by spin coating were transferred onto PDMS stamps. polymer films on PDMS stamps were then stretched to desired strain levels and directly transferred from the PDMS stamp onto the surface of the PEDOT:PSS film. Finally, the residue layers, such as 25 nm TPBi, 1 nm LiF and 100 nm Al, were deposited by thermal evaporating sequentially through a shadow mask at a pressure below 1×10^{-5} mbar.

Mechanical characterizations: Tensile test

The mechanical properties of each polymer film are characterized using tensile tests. Firstly, spin coat a water-soluble sacrificial layer on a 5 mm × 10 mm glass slide. Then spin coat the conjugated polymers onto the sacrificial layer separately. Float each sample on water and transfer the film to a self-made stretching device. Stretch the sample at a strain rate of 0.005 mm s^{-1}.

Crack-on-set strain test

The crack-on-set strain was tested by transferring polymer thin films from OTS substrates onto PDMS. Then the polymer films on PDMS were stretched by using a stretching station and, finally, the crack-on-set strain was monitored by an optical microscope.

Data availability

The datasets generated during and/or analysed during the current study are available in the Figshare repository, [https://doi.org/10.6084/m9.figshare.27431502]. Source data are provided with this paper.

References

1. Su, R. et al. 3D-printed flexible organic light-emitting diode displays. *Sci. Adv.* **8**, eabl8798 (2022).
2. Liu, L. et al. Implantable brain-computer interface based on printing technology. *2023 11th International Winter Conference on Brain-Computer Interface (BCI)* pp. 1–5 (2023).
3. Wei, C. et al. A universal ternary-solvent-ink strategy toward efficient inkjet-printed perovskite quantum dot light-emitting diodes. *Adv. Mater.* **34**, e2107798 (2022).
4. Bai, W. et al. Microscale perovskite quantum dot light-emitting diodes (Micro-PeLEDs) for full-color displays. *Adv. Optical Mater.* **10**, 2200087 (2022).
5. Zhang, P. et al. Integrated 3D printing of flexible electroluminescent devices and soft robots. *Nat. Commun.* **13**, 4775 (2022).
6. Liu, W. et al. High-efficiency stretchable light-emitting polymers from thermally activated delayed fluorescence. *Nat. Mater.* **22**, 737–745 (2023).
7. Zhang, Z. et al. High-brightness all-polymer stretchable LED with charge-trapping dilution. *Nature* **603**, 624–630 (2022).
8. Kim, J. H. & Park, J. W. Intrinsically stretchable organic light-emitting diodes. *Sci. Adv.* **7**, 9715 (2021).
9. Kim, D. C. et al. Three-dimensional foldable quantum dot light-emitting diodes. *Nat. Electron.* **4**, 671–680 (2021).
10. Kwon, J. I. et al. Ultrahigh-resolution full-color perovskite nanocrystal patterning for ultrathin skin-attachable displays. *Sci. Adv.* **8**, eadd0697 (2022).
11. Wei, H. et al. Molecularly engineered host materials for high performance inkjet-printed thermally activated delayed fluorescence organic light-emitting diodes. *J. Mater. Chem. C.* **11**, 4342–4350 (2023).
12. Zhou, L., Yu, M., Yao, L. & Lai, W.-Y. Mayer rod-coated organic light-emitting devices: binary solvent inks, film topography optimization, and large-area fabrication. *Adv. Eng. Mater.* **24**, 2101558 (2022).
13. Minowa, Y. et al. Fast-coating process based on elongated rodlike preaggregate for highly oriented thin film of donor-acceptor pi-conjugated polymer. *ACS Appl. Mater. Interfaces* **14**, 50112–50119 (2022).
14. Cole, C. M. et al. Inkjet-printed self-hosted TADF polymer light-emitting diodes. *Adv. Mater. Technol.* **7**, 2200648 (2022).
15. Yao, Z. F. et al. Ordered solid-state microstructures of conjugated polymers arising from solution-state aggregation. *Angew. Chem. Int. Ed.* **59**, 17467–17471 (2020).
16. Mollinger, S. A. et al. Percolation, tie-molecules, and the microstructural determinants of charge transport in semicrystalline conjugated polymers. *ACS Macro Lett.* **4**, 708–712 (2015).
17. MacFarlane, L. R. et al. Functional nanoparticles through π-conjugated polymer self-assembly. *Nat. Rev. Mater.* **6**, 7–26 (2020).
18. Han, Y. et al. Intrinsically viscoelastic supramolecular conjugated polymer toward suppressing coffee-ring effect. *CCS Chem.* **4**, 3529–3539 (2022).
19. Li, H. et al. Preventing the coffee-ring effect and aggregate sedimentation by in situ gelation of monodisperse materials. *Chem. Sci.* **9**, 7596–7605 (2018).
20. Wang, S. et al. Large-area blade-coated deep-blue polymer light-emitting diodes with a narrowband and uniform emission. *Adv. Sci.* **10**, 2205411 (2022).
21. Lin, J. et al. Ultrastable supramolecular self-encapsulated wide-bandgap conjugated polymers for large-area and flexible electroluminescent devices. *Adv. Mater.* **31**, 1804811 (2019).
22. Yunker, P. J., Still, T., Lohr, M. A. & Yodh, A. G. Suppression of the coffee-ring effect by shape-dependent capillary interactions. *Nature* **476**, 308–311 (2011).
23. Gu, X. et al. The meniscus-guided deposition of semiconducting polymers. *Nat. Commun.* **9**, 534 (2018).
24. Weon, B. M. & Je, J. H. Capillary force repels coffee-ring effect. *Phys. Rev. E* **82**, 015305 (2010).
25. Poulichet, V., Morel, M., Rudiuk, S. & Baigl, D. Liquid-liquid coffee-ring effect. *J. Colloid Interface Sci.* **573**, 370–375 (2020).
26. Hu, H. & Larson, R. G. Marangoni effect reverses coffee-ring depositions. *J. Phys. Chem. B* **110**, 7090–7094 (2006).
27. Dugyala, V. R. & Basavaraj, M. G. Control over coffee-ring formation in evaporating liquid drops containing ellipsoids. *Langmuir* **30**, 8680–8686 (2014).
28. Loudet, J. C., Alsayed, A. M., Zhang, J. & Yodh, A. G. Capillary interactions between anisotropic colloidal particles. *Phys. Rev. Lett.* **94**, 018301 (2005).
29. Raper, J. A. & Amal, R. Measurement of aggregate fractal dimensions using static light scattering. *Part. Part. Syst. Char.* **10**, 239–245 (1993).
30. Liu, B. et al. Improving the intrinsic stretchability of fully conjugated polymer for deep-blue polymer light-emitting diodes with a narrow band emission: benefits of self-toughness effect. *J. Phys. Chem. Lett.* **13**, 7286–7295 (2022).
31. Zhuo, Z. et al. Intrinsically stretchable and efficient fully pi-conjugated polymer via internal plasticization for flexible deep-blue polymer light-emitting diodes with CIE(y) = 0.08. *Adv. Mater.* **35**, e2303923 (2023).
32. Kemerink, M. et al. Relating substitution to single-chain conformation and aggregation in poly(p-phenylene vinylene) films. *Nano Lett.* **3**, 1191–1196 (2003).
33. Abbaszadeh, D. et al. Elimination of charge carrier trapping in diluted semiconductors. *Nat. Mater.* **15**, 628–633 (2016).
34. Noriega, R., Salleo, A. & Spakowitz, A. J. Chain conformations dictate multiscale charge transport phenomena in disordered semiconducting polymers. *Proc. Natl Acad. Sci. USA* **110**, 16315–16320 (2013).
35. Printz, A. D. & Lipomi, D. J. Competition between deformability and charge transport in semiconducting polymers for flexible and stretchable electronics. *Appl. Phys. Rev.* **3**, 021302 (2016).
36. Noriega, R. et al. A general relationship between disorder, aggregation and charge transport in conjugated polymers. *Nat. Mater.* **12**, 1038–1044 (2013).
37. An, X. et al. VPERD assessment of the mechanical property of plasticizing fully π-conjugated polymers with intrinsic stretchability for flexible deep-blue light-emitting diodes. *Adv. Optical Mater.* **12**, 2400010 (2024).
38. Liang, J. J. et al. Elastomeric polymer light-emitting devices and displays. *Nat. Photonics* **7**, 817–824 (2013).

Acknowledgements

This work is financially supported by the National Key R&D Program of China (No. 2020YFA0709900) and the Jiangsu Provincial Senior Talent Program (Dengfeng) (Jiangsu University); W. Huang, J. Lin, B. Liu, L. Bai, and Y. Han acknowledge support from the National Natural Science Foundation of China (No. 62288102, 22075136, 22105099, 62105262, and 62205141) and Funded by Basic Research Program of Jiangsu (BK20243057); Z. Zhuo acknowledge support from the Cultivation Program for The Excellent Doctoral Dissertation of Nanjing Tech University (No.2024-15); L. Sun acknowledge support from the Shenzhen Science and Technology Program (No. RCBS20231211090610014) and China Postdoctoral Science Foundation funded project. We also thank J. Gu from Nanjing University of Science and Technology for his help in theoretical calculations.

Author contributions

M. Ni completed the device preparation, written this manuscript and Supplementary Materials. Z. Zhuo and L. Sun tested the photophysical properties of the material. B. Liu characterized the light scattering

performance of the material and analysed the data. X. An and J. Yang provided assistance in the synthesis of PFPO and POPOF. X. Han and Y. Yang assisted in completing inkjet printing tests. M. Xu, Y. Wu and Q. Feng provided guidance on data analysis. J. Cai provided polymer PODPF. L. Bai checked and organized the data in the article. J. Lin, G. Xie and W. Huang has initiated this project, provided crucial idea and offered enough funds for this work.

Competing interests
The authors declare no competing interests.

Additional information
Supplementary information The online version contains supplementary material available at https://doi.org/10.1038/s41467-024-55494-2.

Correspondence and requests for materials should be addressed to Jinyi Lin or Wei Huang.

Peer review information *Nature Communications* thanks Ebinazar Namdas, and the other, anonymous, reviewer(s) for their contribution to the peer review of this work. A peer review file is available.